Large Near-to-Far Field Spectral Shifts on THz Resonances

Arkabrata Bhattacharya,[1,2,*] Giorgos Georgiou,[1,2] Simon Sawallich,[3]
Christopher Matheisen,[3] Michael Nagel,[3] and Jaime Gómez Rivas[2,4,†]

[1]*FOM Institute AMOLF, P.O. Box 41883 1009 DB Amsterdam, The Netherlands*

[2]*Dutch Institute for Fundamental Energy Research, DIFFER,*
P.O. Box 6336 5600 HH Eindhoven, The Netherlands

[3]*Protemics GmbH, Otto-Blumenthal-Strasse 25 52074 Aachen, Germany*

[4]*Cobra Research Institute, Eindhoven University of Technology,*
Postbus 513, 5600 MB Den Dolech 2, 5612 AZ The Netherlands

(Dated: January 12, 2016)

Abstract

We have performed far-field extinction measurements and near electric field measurements on gold bowtie antennas resonant at THz frequencies. These measurements show a very large shift between the resonant frequencies of the near-field and the far-field spectra. We use the established damped-driven harmonic oscillator model for resonators to model the far-field response of the antennas from the near-field spectrum and show that there is a large discrepancy between the predicted and measured far-field response. We were able to explain this discrepancy by improving the oscillator model with a Fano model. This large shift makes the prediction of the near-field response of resonant structures at THz frequencies very imprecise, provided that only information of the far-field response is available and establishes the necessity of measuring near-fields for a correct and accurate characterization of these structures.

PACS numbers: 73.20.Mf, 68.37.Uv, 78.47.D-, 07.57.Pt

I. INTRODUCTION

When metallic structures are illuminated with electromagnetic radiation, the free charges are driven into a periodic motion following the excitation field. This oscillation of free charges can result into the generation of highly enhanced and confined local electric fields in the vicinity of the structure that are referred to as near-field 'hotspots'[1]. At visible and infrared frequencies the hotspots are caused by localized surface plasmon polaritons or the coherent oscillation of charges in the metallic particle while at lower frequencies these hotspots are the result of surface currents. The generation of these hotspots enables the manipulation of electromagnetic fields in deep sub-wavelength volumes[2–5], which opens up the possibility of imaging and spectroscopy of small objects[6–10]. This concept has been also proposed and demonstrated at THz frequencies[11–15]. Therefore, there is the necessity of optimizing the intensity of confined fields as well as the frequency response for real applications, which is achieved by designing the structure in such a way that it is resonant at the frequency of interest. This resonant behavior is usually characterized with far-field measurements.

Since the interaction of the near-fields with sub-wavelength objects determines the spectral response of the system, it is of utmost importance to characterize the near-field response of the resonant structures. The relation between the near-field response of a structure and its far-field spectrum has been the subject of several studies that have consistently reported a small, yet distinct shift between the near- and far-field resonant frequencies.[16–20]. The origin of this shift is ascribed to the intrinsic damping of the structure and has been modeled using the damped-driven oscillator model[19]. Zuloaga *et al.* have shown that the oscillator amplitude is related to the induced near-field by the surface plasmon polariton and the oscillator dissipated power to the far-field extinction. In a more recent publication by Kats *et al.*[21], it is shown that there are two distinct loss channels by which the localized plasmon mode decays: internal damping via free carrier absorption and emission of radiation or scattering to free space. Using this simple model it was shown that the calculations were in excellent agreement with the numerical simulations in the infrared range. Thus, this result suggests the conjecture that we can accurately predict the near-field spectral response from a far-field measurement, which is intrinsically much easier to perform.

In this manuscript we show experimentally that there can be an anomalously large shift between the near- and far-field resonances, which can not be explained by the oscillator

model. We have performed measurements of the THz near-electric field and of the THz far-field extinction of resonant gold bowtie antennas. Our results show that the frequency shift is comparable to the FWHM of the resonance. Even though our findings are in qualitative agreement with previous studies, the observed spectral shift is significantly larger than what has been previously reported and calculated. We ascribe this discrepancy to the fact that the measured far-field is not just the scattered field from the structures but its interference with the incident field[22]. This spectral interference, described by a Fano model,[23] explains the total response of the system and should be taken into account when designing resonant structures for subwavelength spectroscopy.

II. SAMPLE DESCRIPTION

To study the interaction of THz waves with scattering structures, both in the near- and far-field, we use bowtie antennas made of gold which are designed to resonate at THz frequencies. A bowtie antenna consists of two triangles with pointed tips facing each other and separated by a small gap. These structures are interesting because they combine two distinct electromagnetic effects: the lightning rod effect due to the sharp metallic tips, which leads to high electric field accumulation in the gap and resonant response to the driving field which results from the size and shape of the bowtie. As a result, they do not only create highly enhanced and localized fields in the gap between the two triangles[13,24–27], but also give precise spectral and spatial control over the response with relatively large bandwidths[28]. These structures have been used in the optical range to study effects like single molecule fluorescence[25], two-photon photoluminescence[24],surface-enhanced Raman scattering[29], or as sensors in the THz regime[12].

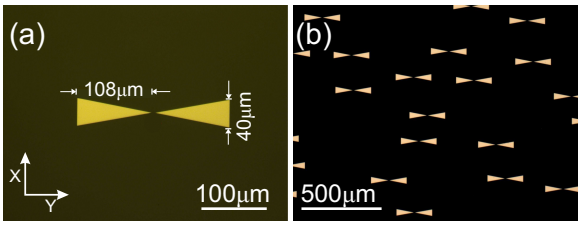

FIG. 1. Optical microscope images of two samples. (a) shows a single bowtie antenna on a quartz substrate, and (b) shows a random array of antennas on a quartz substrate.

The gold antennas were fabricated on quartz substrates using e-beam lithography in combination with standard gold evaporation and lift-off process. Both triangles of the bowtie are 108 μm long with a base of 40 μm each and a gap of 5 μm between them as shown in Fig. 1(a). The bowties are ∼100 nm thick. We have used two different samples: for the near-field measurements, we have fabricated single isolated bowtie structures, as shown in Fig 1(a), to avoid any distortion of the near-field signal by neighboring antennas. For measuring the far-field response we have made a random array of bowties (surface filling fraction 5%) with the same orientation of the long axes, so that all of them are aligned with the polarization of the driving THz field. A microscope image of the sample used for the far-field measurements is shown in Fig. 1(b). This random ensemble increases the signal to noise in the extinction measurements[30] but, as we show later it also defines the interference path that gives rise to a large discrepancy between the near- and far-field responses of the sample. In a random array, as shown in Fig. 1(b), there can be two different kind of coupling effects between neighbouring structures. First is the radiative or far-field coupling due to scattered field from the nearby structures. Due to random distribution of the bowtie antennas in the array, the phase relation between the scattered fields is averaged, and the effect due to radiative coupling cancels out. We have measured the extinction at different locations on the sample obtaining always the same result within the accuracy of the measurements. The other coupling effect is due to near-field coupling between adjacent antennas due to spatial overlap of the local fields. This coupling is minimized by placing the antennas sufficiently far from each other.

The measurement of the near-field spectrum was done with a THz near-field micro-spectroscopy setup. This setup is driven by a femtosecond IR oscillator, which operates at 800 nm with a pulse duration of 20 fs and repetition rate of 80 MHz. This train of pulses is divided into two beams: the first beam carrying most of the power (∼350 mW) goes through a delay stage and is incident on a photoconductive antenna which generates the THz radiation[31]. The THz radiation is weakly focussed onto the sample by a pair of gold off-axis parabolic mirrors. The other beam carrying a little amount of power (∼5 mW) is used for biasing the probe-tip[32] used for the near-field measurements. This tip is a small photo-conductive antenna of 10 μm^2, that measures the electric field amplitude by the principle of photo-conductive sampling[33]. For each temporal position in the THz transient the tip generates a proportional current, which is amplified and measured using a lock-in

detection. By changing the path length of the THz generation beam with the delay stage the whole THz transient is probed, and thus the electric field in the near-field of the sample is measured. The measurements are polarization sensitive, i.e., they depend on the orientation of the probe with respect to the incident THz. The sample is mounted on a combination of three linear stages, making it possible to measure the local fields at all points above the sample.

In the setup for measuring the far-field, the generation of THz is done using the same technique as mentioned previously. However, the detection of THz radiation is done by a conventional electro-optic THz sampling technique[34,35] using the THz field amplitude induced birefringence of a non-linear ZnTe crystal.

III. EXPERIMENTAL RESULTS

We define two quantities for comparing the near-field to the far-field measurements. First, the near-field intensity spectrum, $\mathcal{S}_{NF}$, of the bowtie antenna is defined as, $\mathcal{S}_{NF}(\overline{r},\nu) = \left|\frac{E^{NF}(\overline{r},\nu)}{E^{NF}_{ref}(\overline{r_0},\nu)}\right|^2$, where $E^{NF}(\overline{r},\nu)$ is the electric near-field at frequency ν and position $\overline{r}$ in the proximity of the bowtie antenna and $E^{NF}_{ref}(\overline{r_0},\nu)$ is the electric field at the same height and frequency but at a position away from the antenna. For now, we define this quantity at the gap between the triangles of the antenna. The second quantity is the far-field extinction spectrum, $\mathcal{S}_{FF}$, of the sample. The extinction is defined as $\mathcal{S}_{FF}(\nu) = 1 - \left|\frac{E^{FF}(\nu)}{E^{FF}_{ref}(\nu)}\right|^2$, where $E^{FF}(\nu)$ is the transmitted electric field through the sample with the random array of the bowtie at frequency ν and $E^{FF}_{ref}(\nu)$ is the transmitted field without the bowties, i.e. the bare substrate.

The measured near- and the far-field spectra are shown in Fig. 2. The triangles represent the near-field spectrum in the gap of the single bowtie antenna at a height of 1 μm above the substrate and the circles correspond to the far-field extinction of the random array of bowtie antennas. Both spectra show a resonant behavior but not at the same frequencies. For the near-field spectrum, the resonant frequency is at 0.62 THz. The far-field spectrum is remarkably blue-shifted from the near-field, with the resonant frequency at 0.85 THz. As it is discussed in the following section, the observed shift in our measurements can not be explained by the extensively used driven-damped oscillator model that approximates the

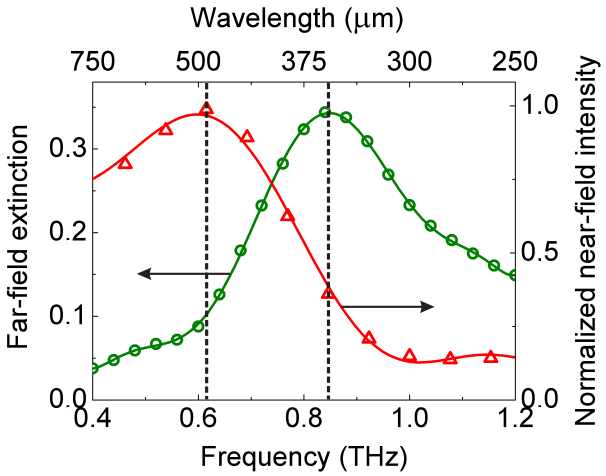

FIG. 2. Near-field spectrum measured at the gap of a gold bowtie antenna (red triangles) and far-field extinction spectrum (green circles). The solid curves are guides to the eye. The vertical dashed lines indicate the resonant frequencies in the near- and far-field.

response of the bowtie.

To investigate the spectral properties of the near-field around the bowtie antennas, we have measured spatial maps of the near-field at two different frequencies marked by the dotted lines in Fig. 2. The first line at 0.62 THz indicates the resonant frequency of the near-field and the second line at 0.85 THz corresponds to the resonant frequency of the far-field spectrum. Figure 3 shows the spatial maps of near-field intensities around the bowtie antenna at these frequencies. The color scale is kept the same in both the measurements to facilitate a direct comparison. These measurements show the local intensity enhancement in the gap of the bowtie at 0.62 THz (Fig. 3(a)). The sharp tips give rise to localized electromagnetic fields, whereas the spectral resonance due to the dimensions of the bowtie enhances these fields. The field is pronouncedly less enhanced at 0.85 THz (Figure 3(b)) in spite of this being the resonant frequency of the far-field.

IV. NUMERICAL SIMULATIONS

We have performed numerical simulations using the Finite-Difference in Time-Domain method (FDTD) to model the response of a single bowtie antenna. Since gold is a very good conductor at THz frequencies we can approximate the material as a perfect electric conductor. We have verified the validity of this approximation which neglects the penetra-

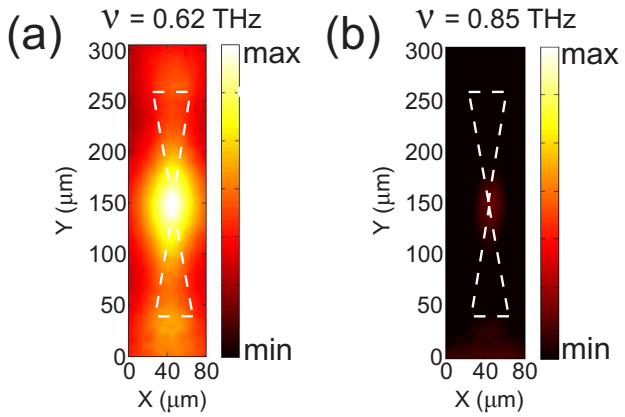

FIG. 3. (a) Electric field intensity map measured at 0.62 THz and at a height of 1 μm above the bowtie antenna.(b) Electric field intensity map at 0.85 THz and the same height. The color scales are kept the same on both figures. In both panels the dashed lines indicate the boundaries of the bowtie antenna.

tion of the electromagnetic field in the metal and simplifies the simulations significantly. The excitation is done with a broadband THz source similar to the experiments. The simulation volume contains a single bowtie antenna and the boundary conditions are perfectly impedance matched layers to the surroundings. Both the near-field and the far-field of the bowtie are calculated by referencing the power of the total field by the power of the total field without the antenna. Similar to the experiments, the illumination is done from the side of the quartz substrate.

We have simulated the far-field extinction spectrum and the near-field intensity spectrum at a height of 1 μm above the antenna and at the center of the gap. Figure 4(a) displays the measured near-field (open circles) together with the simulation (solid curve). The experimental data and the simulation results are in a excellent agreement. From this result we can conclude that the probe-tip used for the measurements does not perturb the near-fields significantly. The inset of Fig. 4(a) illustrates the near-field intensity map at the resonance frequency of 0.62 THz. The maximum enhancement in the near-field intensity is, as expected, in the gap. Figure 4(b) shows the measurements (open circles) and the simulations (solid curve) of the far-field extinction, illustrating also the excellent agreement between the measurement and the simulation. The small discrepancy at high frequencies is most likely due to the fact that the experiments were performed with a weakly focussed beam, whereas in the simulations a perfect collimated beam is used.

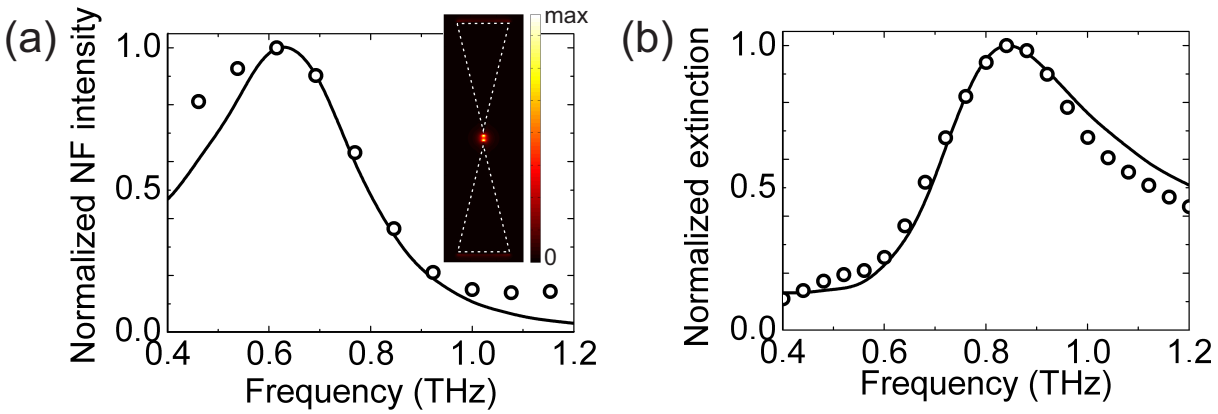

FIG. 4. (a) The circles represent the measured near-field spectrum of the bowtie antenna on the gap between the two triangles at a height of 1 μm, while the solid black curve is the simulated spectrum. The inset shows the near-field intensity map at 0.62 THz.(b) The circles represents the extinction spectrum of the random array of bowtie antennas and the solid black curve is the simulated far-field extinction spectrum.

V. DRIVEN-DAMPED HARMONIC OSCILLATOR MODEL

The relation between the near- and the far-field response of resonant metallic structures has been approximated in the literature by a driven-damped harmonic oscillator model. This analogy is often justified by the fact that the dynamics of free electrons in a conducting structure under the influence of a driving electric field follows an harmonic oscillation which is damped by Ohmic losses in the metal and by radiation damping from the accelerated charges. The resonant nature of the harmonic oscillator is determined primarily from the geometry of the structure. The oscillatory motion of the electrons in the bowtie can be affected due to the capacitive coupling between the two resonant elements of the bowtie antenna, i.e., the gold triangles. A comparison between the simulations of individual triangles of the bowtie (not shown here) with the whole bowtie structure establishes that although there is a weak coupling between the triangles of the bowtie, both responses are similar. Thus, without the loss of generality we can approximate the bowtie antenna as a single damped oscillator.

The spectral amplitude of the near-field close to the gap of the bowtie depends on the localization of charges accumulated at the two tips of the bowtie structure. Due to the symmetry of the structure, we can assume that both charge distributions are the same. Using the model described in Refs. [18] and [21] we can describe the motion of free charges

using the equation of motion of a damped harmonic oscillator,

$$\frac{d^2Q}{dt^2} + 2\pi\nu_0\Gamma_a\frac{dQ}{dt} + (2\pi\nu_0)^2Q = A_0(\nu)e^{-2\pi i\nu t} + 2\pi\nu_0\Gamma_s\frac{d^3Q}{dt^3} \tag{1}$$

where $Q(\nu,t)$ is the charge distribution as a function of time, $A_0(\nu)$ is the harmonic driving field, ν_0 is the natural frequency of the oscillator, Γ_a is the internal damping constant and $\Gamma_s = (1/\nu_0)Q_{tot}^2/6\pi\epsilon_0 c^3$ is the radiation reaction coefficient also known as Abraham-Lorentz force, which represents the force that the free charges feel when they emit radiation[36]. The $1/\nu_0$ term is a scaling factor and Q_{tot} is the total number of free charges contributing to the damped oscillation. The value of Q_{tot} is estimated from the number of free electrons present in the structure, which is calculated by taking into account the free-electron density of gold ($\mathcal{N}_{Au} = 5.9 \cdot 10^{22}\text{cm}^{-3}$). The harmonic charge oscillation is determined by solving Eq. (1) and is given by,

$$Q(\nu,t) = \sqrt{\mathcal{S}_{NF}(\nu)}e^{-i(2\pi\nu t + \phi(\nu))}, \tag{2}$$

where,

$$\mathcal{S}_{NF}(\nu) = \left|\frac{1}{\sqrt{(2\nu\nu_0(\Gamma_a + \nu^2\Gamma_s))^2 + (\nu^2 - \nu_0^2)^2}}\right|^2 \tag{3}$$

is the frequency dependent near-field intensity response with $\Gamma_a + \nu^2\Gamma_s$ as the frequency dependent damping term, and $\phi(\nu)$ is the corresponding phase response of the damped harmonic oscillator, both referenced with respect to the source.

From the fits of the calculated $\mathcal{S}_{NF}(\nu)$ to the near-field measurements as shown in Fig. 5(a), we can extract the natural frequency and damping constant of the oscillator, which are $\nu_0 = 0.683 \pm 0.004$ THz and $\Gamma_a = 0.302 \pm 0.018$, respectively. With these values the harmonic oscillator model fits excellently the experimental near-field intensity.

The time averaged scattered and absorbed power spectra of the oscillator can be calculated using the following expressions,[21]

$$P_{abs}(\nu) = \nu^2\nu_0\Gamma_a\mathcal{S}_{NF}(\nu), \tag{4}$$

$$P_{scat}(\nu) = \nu^4\nu_0\Gamma_s\mathcal{S}_{NF}(\nu). \tag{5}$$

These spectra are shown in Fig. 5(b) with a dashed (absorption) and dotted (scattering) red curves, where we can appreciate that both the absorption and scattering spectra are

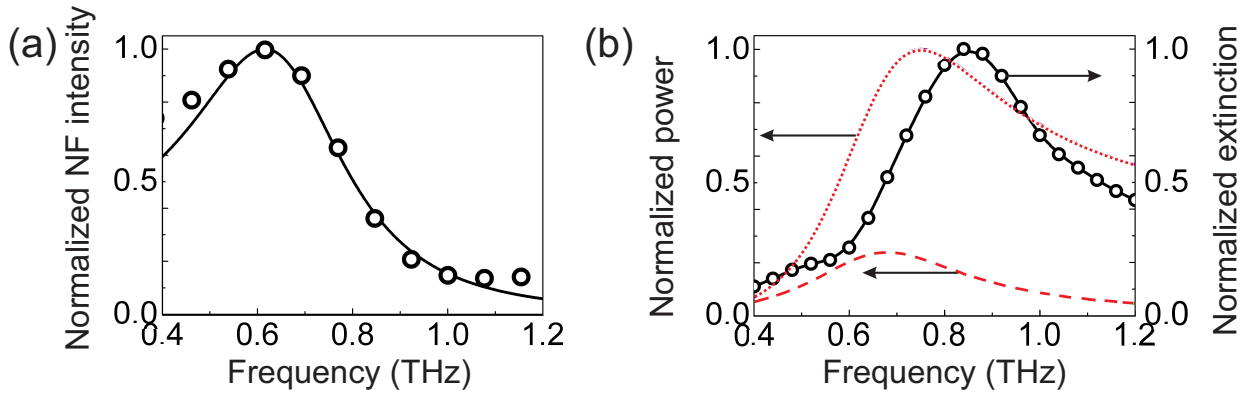

FIG. 5. (a) The open circles represent the measured normalized near-field intensity, while the solid line is the fit to the measurements using the damped oscillator model. (b) Absorption and scattering spectral powers calculated from the harmonic oscillator model using the same parameters as in (a). The red dotted curve shows the scattering spectrum and the absorption spectrum is shown by the red dashed curve. Both the scattering and the absorption spectra have been normalized to the maximum of the scattering spectrum. The absorption spectrum is multiplied by a factor of 10 after normalization to elucidate its spectral response. The black line with circles represents the measured extinction spectrum from the random bowtie sample normalized to its maximum.

blue-shifted with respect to the near-field intensity spectrum. The absorption spectrum peaks at the natural frequency of 0.68 THz, whereas the peak of the scattering spectrum is around 0.75 THz. These kind of shifts between scattering and absorption spectrum has been experimentally as well as theoretically reported in several articles[37–39]. The use of a good conductor at THz frequencies is manifested by the fact that the spectral absorption is far lesser than the scattering. Gold behaves close to a perfect electric conductor in this frequency range and the absorption is low. Thus, we can conclude that the extinction spectrum of these structures in the far-field is dominated by scattering. This dominant scattering at THz frequencies makes the resonance of the extinction spectra significantly blue shifted from the resonance of the near-field as compared to similar measurements with gold at optical frequencies, where the effect of absorption in extinction is comparable to the scattering.

If we compare both the measured extinction (black circles in Fig. 5(b)) and the calculated scattering (red dotted line), we see a discrepancy in the resonant frequencies. The resonance of the scattering spectrum is at 0.75 THz, whereas the resonance of the extinction spectrum

is at 0.85 THz. A quantitative description of this discrepancy is given in the next section.

VI. FANO MODEL

In order to explain the discrepancy between the experimental extinction and the oscillator model, we need to consider the incident field in the extinction: The incident field that is not perturbed by the bowtie, interferes with the scattered far-field defining the extinction. This interference, which is not considered by the simple harmonic oscillator model, is the origin of the discrepancy between this model and the extinction measurements. The interference can be described with a Fano model[23,40], which defines a distinctly asymmetric line-shape with the functional form

$$F(\nu) = \frac{(q\nu_D\Gamma + \nu - \nu_D)^2}{(\nu - \nu_D)^2 + \nu_D^2\Gamma^2}, \tag{6}$$

where ν_D and Γ are the frequency and line-width of a discrete state with a Lorentzian resonance profile that interferes with a continuum. The phenomenological shape parameter, q, is defined as the ratio between spectral amplitude of the discrete state and the continuum. In the limit $|q| \to \infty$ the resonance is dominated by the lineshape of the discrete state (Lorentzian resonance), whereas at values close to unity ($q \sim 1$) the discrete state and the continuum have equal strengths and the resonance profile shows an asymmetric lineshape similar to the one observed in the far-field extinction spectrum of the bowtie antennas (Fig. 2).

Fano resonances in single scatteres have been described in the literature to arise form different sources like coupling between spatially and spectrally overlapping adjacent bright and dark modes[37], coupling between resonant modes with induced image charges in substrates with high dielectric constant[41], from systems with broken symmetries[42], or between odd parity modes of single nano rods and background continuum[43]. However, the source of the Fano resonance discussed here is not only coupling of a broad continuum to a sharp resonant mode due to a single particle, but also the presence of many particle, which boosts the signal strength of the interference channel of the resonant mode and thereby reshaping the response of the system.

In the far-field extinction measurements the measured quantity is the total field, which corresponds to the interference of the scattered (discrete state representing the oscillator) and the incident field (continuum). Therefore, it is expected that these fields give rise

to a Fano-like resonance: the interference pathway being the sharp radiant dipolar mode which is resonantly scattered by the bowties and the fraction of the incident THz field which is unperturbed (unscattered) forming the broad continuum. This gives rise to a distinct asymmetry in the lineshape of the extinction and a consequent shift of the resonant frequency from the Lorentzian resonant profile. This pronounced shift of the resonance frequency depends on the relative strength of the incident field in the interference effect.

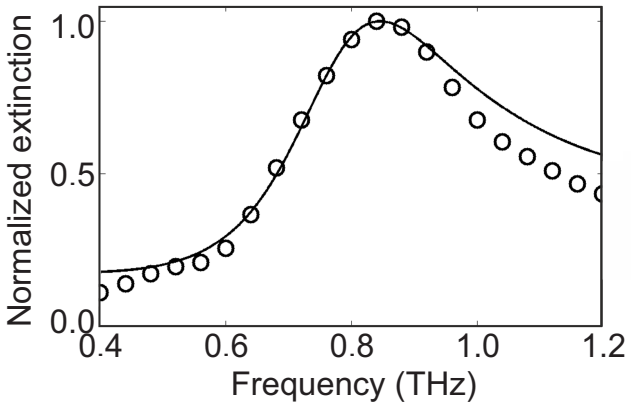

FIG. 6. The black circles represent the measured and normalized extinction spectrum, while the solid line is a fit to the measurements using the Fano model.

To verify the asymmetric nature of the far-field resonance and the consequent shift of extinction peak from calculated values, we have fit Eq.(6) to the measured extinction spectrum using the parameters extracted from the fit of the oscillator model to the near-field intensity spectrum, i.e., $\nu_D = 0.75$ THz (the resonant frequency of the scattering spectrum) and $\Gamma = (\nu_0/\nu_D)(\Gamma_a + \nu^2\Gamma_s)$ (the frequency dependent damping term from the oscillator model with proper scaling factor) with q=2.02±0.05 as the only fit parameter. This result is shown in Fig. 6, where the circles illustrate the far-field extinction measurements and the solid curve is the fit. The small deviation of the fit at high frequencies can be attributed to the approximation of the broad THz source as a continuum. Since the source spectrum has a limited bandwidth, at higher frequencies its approximation to the continuum becomes increasingly imprecise.

The relatively low value of q obtained from the fit indicates that the transmitted unperturbed field amplitude is marginally smaller than the scattered field by the bowtie. With this value of q the large shift of the resonant frequency in the experiments can be explained.

The shift depends on several factors: The most important one is the ratio between the total spectral powers integrated over all frequencies of the scattered and the incident fields. The filling fraction of the bowtie antennas forming the sample also determines the ratio of the scattered to incident fields, and as a result, contributes to this Fano-like resonance. In order to reduce the asymmetry in the Fano-like lineshape it is possible to increase the density of the bowties, i.e. increase the fraction of scattered intensity relative to the incident THz intensity. The far-field spectrum depends not only on the size and shape of the resonant structures and on their surface filling fraction of the sample, but also on the properties of the incident field.

The model presented above should be valid in all frequency ranges provided that material resonances are far from the spectral window of interest. However, this spectral interference effect should not affect substantially the spectrum of the near-fields in the confined hotspots mostly due to the fact that the electric fields in these regions are enhanced with respect to the incident field amplitude, hence approximating the condition $q \to \infty$. In this limit, the spectrum is dominated by the lineshape of the near-field and the measured near-field resonance will be at the same frequency as the predicted resonance by the oscillator model. These results establishes the necessity of measuring the near-field for an accurate characterization of resonant structures.

VII. CONCLUSIONS

We have shown that the far-field extinction spectrum of resonant structures at THz frequencies can have very large spectral blue-shifts with respect to the near-field intensity spectra. These shifts can be comparable to the FWHM of the resonance and can not be solely attributed to the intrinsic nature of the structures. Rather, the incident field plays an important role in defining the far-field spectral response of these structures. The large shifts can be explained analytically by using a Fano model that improves the driven-damped harmonic oscillator model extensively used to describe these structures. An important consequence of these results is that the characterization of resonant structures based solely on their far-field response can lead to misleading results that suggest field enhancements at frequencies at which the near-field is not changed significantly. Therefore, near-field measurements are necessary for an accurate description of resonant structures.

ACKNOWLEDGMENTS

The authors thank Gopika Ramanandan and Martijn Schaafsma for valuable discussions and for assistance in the experiments, Peter Govers and Dimitry Lamers for fabricating the samples and Niels Commandeur, Luc Blom, Jan Versluis, Duncan Verheijde and Iliya Cerjak for technical support. We thank the financial support of ERC through grant no 259272 THZ-PLASMON and the Foundation for Fundamental Research on Matter (FOM), which is part of the Netherlands Organization for Scientific Research (NWO).

---

* A.Bhattacharya@amolf.nl

† J.Gomez@amolf.nl

[1] H. Xu, J. Aizpurua, M. Käll, and P. Apell, Phys. Rev. E **62**, 4318 (2000).

[2] J. R. Krenn, A. Dereux, J. C. Weeber, E. Bourillot, Y. Lacroute, J. P. Goudonnet, G. Schider, W. Gotschy, A. Leitner, F. R. Aussenegg, and C. Girard, Phys. Rev. Lett. **82**, 2590 (1999).

[3] M. L. Brongersma, J. W. Hartman, and H. A. Atwater, Phys. Rev. B **62**, R16356 (2000).

[4] S. A. Maier, M. L. Brongersma, P. G. Kik, S. Meltzer, A. A. G. Requicha, and H. A. Atwater, Advanced Materials **13**, 1501 (2001).

[5] F. Svedberg, Z. Li, H. Xu, and M. Käll, Nano Letters **6**, 2639 (2006).

[6] E. Betzig, A. Harootunian, A. Lewis, and M. Isaacson, Appl. Opt. **25**, 1890 (1986).

[7] F. J. García-Vidal and J. B. Pendry, Phys. Rev. Lett. **77**, 1163 (1996).

[8] K. Kneipp, Y. Wang, H. Kneipp, L. T. Perelman, I. Itzkan, R. R. Dasari, and M. S. Feld, Phys. Rev. Lett. **78**, 1667 (1997).

[9] F. Neubrech, A. Pucci, T. W. Cornelius, S. Karim, A. García-Etxarri, and J. Aizpurua, Phys. Rev. Lett. **101**, 157403 (2008).

[10] J. P. Camden, J. A. Dieringer, J. Zhao, and R. P. Van Duyne, Accounts of Chemical Research **41**, 1653 (2008).

[11] M. A. Seo, H. R. Park, S. M. Koo, D. J. Park, J. H. Kang, O. K. Suwal, S. S. Choi, P. C. M. Planken, G. S. Park, N. K. Park, Q. H. Park, and D. S. Kim, Nat Photon **3**, 152 (2009).

[12] A. Berrier, P. Albella, M. A. Poyli, R. Ulbricht, M. Bonn, J. Aizpurua, and J. G. Rivas, Optics Express **20**, 5052 (2012).

[13] A. Berrier, R. Ulbricht, M. Bonn, and J. G. Rivas, Opt. Express **18**, 23226 (2010).

[14] V. Giannini, A. Berrier, S. A. Maier, J. A. Sánchez-Gil, and J. G. Rivas, Opt. Express **18**, 2797 (2010).

[15] L. Razzari, A. Toma, M. Shalaby, M. Clerici, R. P. Zaccaria, C. Liberale, S. Marras, I. A. I. Al-Naib, G. Das, F. D. Angelis, M. Peccianti, A. Falqui, T. Ozaki, R. Morandotti, and E. D. Fabrizio, Opt. Express **19**, 26088 (2011).

[16] V. Giannini, G. Vecchi, and J. Gómez Rivas, Phys. Rev. Lett. **105**, 266801 (2010).

[17] P. Alonso-González, P. Albella, F. Neubrech, C. Huck, J. Chen, F. Golmar, F. Casanova, L. E. Hueso, A. Pucci, J. Aizpurua, and R. Hillenbrand, Phys. Rev. Lett. **110**, 203902 (2013).

[18] C. A. Werley, K. Fan, A. C. Strikwerda, S. M. Teo, X. Zhang, R. D. Averitt, and K. A. Nelson, Opt. Express **20**, 8551 (2012).

[19] J. Zuloaga and P. Nordlander, Nano Letters **11**, 1280 (2011).

[20] C. Menzel, E. Hebestreit, S. Mühlig, C. Rockstuhl, S. Burger, F. Lederer, and T. Pertsch, Opt. Express **22**, 9971 (2014).

[21] M. A. Kats, N. Yu, P. Genevet, Z. Gaburro, and F. Capasso, Opt. Express **19**, 21748 (2011).

[22] P. Fan, Z. Yu, S. Fan, and M. L. Brongersma, Nat Mater **13**, 471 (2014).

[23] U. Fano, Phys. Rev. **124**, 1866 (1961).

[24] P. J. Schuck, D. P. Fromm, A. Sundaramurthy, G. S. Kino, and W. E. Moerner, Phys. Rev. Lett. **94**, 017402 (2005).

[25] A. AU Kinkhabwala, Z. Yu, S. Fan, Y. Avlasevich, K. Mullen, and W. E. Moerner, Nat Photon **3**, 654 (2009).

[26] T. Hanke, J. Cesar, V. Knittel, A. Trgler, U. Hohenester, A. Leitenstorfer, and R. Bratschitsch, Nano Letters **12**, 992 (2012).

[27] A. Singh, G. Calbris, and N. F. van Hulst, Nano Letters **14**, 4715 (2014).

[28] H. Fischer and O. J. F. Martin, Opt. Express **16**, 9144 (2008).

[29] D. P. Fromm, A. Sundaramurthy, A. Kinkhabwala, P. J. Schuck, G. S. Kino, and W. E. Moerner, The Journal of Chemical Physics **124**, 061101 (2006).

[30] M. C. Schaafsma, H. Starmans, A. Berrier, and J. G. Rivas, New Journal of Physics **15**, 015006 (2013).

[31] E. R. Brown, F. W. Smith, and K. A. McIntosh, Journal of Applied Physics **73**, 1480 (1993).

[32] M. Wächter, M. Nagel, and H. Kurz, Applied Physics Letters **95**, 041112 (2009).

[33] J. Kim, S. Williamson, J. Nees, S. Wakana, and J. Whitaker, Applied Physics Letters **62**, 2268 (1993).

[34] Q. Wu and X.-C. Zhang, Applied Physics Letters **67**, 3523 (1995).

[35] A. Nahata, A. S. Weling, and T. F. Heinz, Applied Physics Letters **69**, 2321 (1996).

[36] D. J. Griffiths, *Introduction to Electrodynamics*, 3rd ed. (Benjamin Cummings, New York, 1999).

[37] S. Zhang, L. Chen, Y. Huang, and H. Xu, Nanoscale **5**, 6985 (2013).

[38] A. Losquin, L. F. Zagonel, V. Myroshnychenko, B. Rodrguez-Gonzlez, M. Tenc, L. Scarabelli, J. Förstner, L. M. Liz-Marzn, F. J. G. de Abajo, O. Stphan, and M. Kociak, Nano Letters **15**, 1229 (2015).

[39] A. Losquin and M. Kociak, ACS Photonics **2**, 1619 (2015).

[40] A. E. Miroshnichenko, S. Flach, and Y. S. Kivshar, Rev. Mod. Phys. **82**, 2257 (2010).

[41] H. Chen, L. Shao, T. Ming, K. C. Woo, Y. C. Man, J. Wang, and H.-Q. Lin, ACS Nano **5**, 6754 (2011).

[42] N. W. Bigelow, A. Vaschillo, J. P. Camden, and D. J. Masiello, ACS Nano **7**, 4511 (2013).

[43] N. Verellen, F. Löpez-Tejeira, R. Paniagua-Domnguez, D. Vercruysse, D. Denkova, L. Lagae, P. V. Dorpe, V. V. Moshchalkov, and J. A. Sánchez-Gil, Nano Letters **14**, 2322 (2014).